ELSEVIER

Journal of Power Sources 58 (1996) 73–78

JOURNAL OF POWER SOURCES

Electrochemical behaviour of multicomponent Zr–Ti–V–Mn–Cr–Ni alloys in alkaline solution

Grażyna Wójcik [a], Maciej Kopczyk [a], Grażyna Młynarek [a], Włodzimierz Majchrzyckia [a], Maria Bełtowska-Brzezinska [b,*]

[a] *Centralne Laboratorium Akumulatorów i Ogniw, Forteczna 12/14, 61-362 Poznań, Poland*

[b] *Faculty of Chemistry, A. Mickiewicz University, Grunwaldzka 6, 60-780 Poznań, Poland*

Received 23 June 1995; revised 22 November 1995; accepted 28 November 1995

Abstract

The effect of the composition of multicomponent Zr–Ti–V–Mn–Cr–Ni alloys on their hydrogen-storage capacity and on the rate of electrosorption/desorption of hydrogen was investigated under potentiodynamic as well as single-pulse and long-term galvanostatic conditions. The main characteristics of alloys and alloy electrodes were determined by their structural analysis by means of X-ray diffraction and scanning electron microscope, by specific surface area tests and by determination of the hydrogen absorption/desorption isotherms in the gas/solid phase system. It was found that only the alloys with a manganese content below a threshold could be used as electrode materials for Ni–MH batteries, whereas the modification of the electrode material by micro-encapsulation of alloy particles should limit the dissolution of manganese from the electrode material in a strong alkaline solution.

Keywords: Alloys; Zirconium; Titanium; Vanadium; Manganese; Chromium; Nickel; Alkaline solution

1. Introduction

The AB_2-type multicomponent alloys belonging to the Laves phase system display a high hydrogen-storage capacity. A possibility of large differentiation of their composition enables to employ a comprehensive raw material base. This is the reason why these alloys are the subject of interest for use as the electrode material in Ni–MH batteries. Venkatesan, Fetcenko and co-workers [1,2] reported an increased hydrogen-storage capacity of alloy electrodes made of AB_{2+x}-type nonstoichiometric alloys and moreover discharge capability was shown to be higher for the sintered electrodes than for the compressed ones. The purpose of this work was to investigate the influence of the composition of this type of alloys on the dynamics of electrochemical hydrogen absorption/desorption, as well as on electrode capacity in charge/discharge cycles, in order to select alloys of electrochemically and economically advantageous composition.

2. Experimental

The nonstoichiometric alloys of AB_{2+x}-type were obtained by melting metallic components (99.9% purity Merck) at an appropriate quantitative ratio in an arc furnace in an argon atmosphere. Thereafter, the alloys obtained were disintegrated by hydrogen absorption and desorption from the gas phase.

The working electrodes were prepared from pulverized alloys of 0.03–0.08 mm granulation with addition of 5% nickel powder (Ni 255, Inco) in the form of pressure formed tablets placed in a basket made of fine nickel wire mesh as the current collector. Electrodes of increased mechanical resistivity were obtained by sintering inside a quartz tube for 15 min at $T = 1223 \pm 10$ K in a argon stream with a 4% addition of hydrogen [3]. Etching of the tested electrodes in hot 6 M KOH solution at $T = 373$ K was sufficient for the initial activation.

All electrochemical measurements were carried out in a three-compartment glass cell with the Hg/HgO/6 M KOH reference electrode and the large surface $NiOOH/Ni(OH)_2$ auxilliary electrode. The cell was filled with an air-free 6 M KOH solution prepared from analar grade KOH (POCH Gliwice, Poland) in double-distilled water, at 293 K.

In studies of the electrochemical absorption/desorption of hydrogen on the investigated alloys, the potentiodynamic and galvanostatic methods were employed, as described in Ref. [4]. The apparatus consisted of a 20A ELPAN potentiostat,

* Corresponding author.

SSDI 0378-7753(95)02325-9

an EG 20 ELPAN wave generator, a galvanostat made in the Central Laboratory of Cells and Storage Batteries (Poznań) and an x–y recorder Rihen Denishi.

The charge-transfer resistance and the mass-transfer resistance were determined from the overpotential versus time transients recorded during the galvanostatic pulse for alloy electrodes after chemical activation as well as for electrodes charged to the potential of hydrogen evolution and discharged down to −0.750 V versus Hg/HgO/6 M KOH after having reached the equilibrium potential. In the continuous charge/discharge cycles, the electrodes were charged and discharged at different constant-current density (j = constant) values in the same potential range. The relaxation time between successive charge/discharge cycles was 30 min, sufficient to reach the equilibrium potential for all investigated electrodes.

The potentiodynamic measurements of the current density versus overpotential (j–η) were carried out at the potential sweep within 1 to 100 mV s^{-1} for the electrodes at the charge state identical to that in the galvanostatic measurements.

In the measurements of the electrochemical absorption/desorption isotherms of hydrogen, the electrodes were charged and discharged at j = constant using intermittent mode of operation with relaxation periods at open circuit. The hydrogen-storage capacity of an electrode was calculated from the charge released during the discharge, as the amount of wt. % of hydrogen absorbed on one mole of the alloy. The hydrogen-equilibrium pressure was calculated using the Nernst equation [5].

The capability of the alloy electrodes of charge retention was estimated after 25 charge/discharge cycles and after storing the charged electrode for 30 days at T = 298 K and then discharged to −0.750 V versus the Hg/HgO/6 M KOH.

Structural changes of the electrode material were checked by the X-ray diffraction method using Cu Kα lines as well as with the scanning electron microscope (SEM) Jeol, JSM 50A-type with electronic probe microanalysis (EPMA) JXA 50A, WDS-type. The specific surface of the electrode material was obtained by the BET method using the ASAP 2010 M, Micromerilitic.

The hydrogen absorption/desorption (p–c) isotherms in the gas/solid-phase system were determined with the Sievert-type apparatus at room temperature.

3. Results and discussion

Compositions of the nonstoichiometric alloys of the AB_{2+x}-type investigated in this work are listed in Table 1. In alloy I vanadium was completely replaced by manganese, in alloys II, III, IV and V only partially. In the case of alloys IV and V, the atomic ratio Ti:Zr was changed from 2:1 for alloy IV to 1:1 for alloy V.

Table 1
Composition of multicomponent alloys

Alloy	Atomic %					
	Zr	Ti	V	Mn	Cr	Ni
I	10.08	19.19		24.82	7.74	38.17
II	10.08	19.19	5.88	18.94	7.74	38.17
III	10.08	19.19	11.76	13.06	7.74	38.17
IV	10.08	19.19	17.64	7.18	7.74	38.17
V	14.64	14.64	17.64	7.18	7.74	38.17

3.1. Physicochemical characteristics of the investigated alloys

X-ray structural (XRD) analysis of alloys IV to V indicated the existence of lines characteristic for the C14 Laves phase and other lines of small intensity. The use of SEM/EPMA made it possible to identify an additional phase existing in the amount below 0.5% as a solid solution of vanadium and chromium. In alloy V, for example, it consisted of 9.93 at.% Mn, 31.35 at.% Cr, 45.75 at.% V, 5.76 at.% Ni, 1.46 at.% Ti, 5.76 at. % Zr. The presence of the additional phase next to the C14 main phase in the overstoichiometric alloys of the AB_{2+x} was also noticed previously by Miyamura et al. [6].

An increase in the unit cell volume of the virgin alloy caused by hydrogen absorption, manifested by a shift of the diffraction lines characteristic of the Laves phase in the direction of smaller angles, proves that the hydrogen atoms are built in the alloy crystal lattice forming hydrides. For example, the unit cell volumes for the virgin alloys IV and V are equal to 165.5 and 169.5 Å^3, respectively, and for the same alloys after absorption and desorption of hydrogen from the gas phase 166.9 and 170.45 Å^3, respectively. The changes in crystal lattice parameters concomitant with the electrochemical hydrogen absorption and desorption are illustrated in Fig. 1. One can see that the unit cell volume for charged electrodes increases but in the case of the discharged electrodes it is again comparable with that of the virgin alloy. No changes of structural parameters were found for discharged electrodes after 10 charge/discharge cycles. XRD in situ

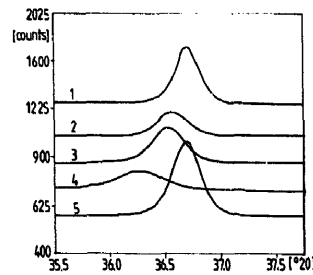

Fig. 1. X-ray diffraction patterns (110) for alloy IV: (1) virgin alloy; (2) after hydrogenation from the gas phase; (3) after 4 h activation in 6 M KOH at T = 373 K; (4) for electrode material in charged state, and (5) electrode material in discharged state.

measurements during the electrode charge and discharge should reveal more substantial information on the structural changes in the electrode material during the cyclic operation of electrode.

The alloys disintegrate during the initial chemical activation as well as in the successive charge/discharge cycles, which is manifested as an increase in the specific surface area of the electrode material, i.e. for alloy IV from 0.89 to 1.96 $m^2 g^{-1}$ after chemical activation and to 7.92 $m^2 g^{-1}$ after 15 charge/discharge cycles, for alloy V from 0.87 to 1.25 $m^2 g^{-1}$ after chemical activation and to 3.42 $m^2 g^{-1}$ after 15 charge/discharge cycles.

3.2. Electrochemical characteristics of Zr–Ti–V–Mn–Cr–Ni alloys in alkaline solution

3.2.1. Chemical activation of alloys

Following the literature reports [7,8], chemical activation of alloy electrodes was carried out in order: (i) to modify the structure of the oxide layer formed on an alloy granule as a result of contact with air, and (ii) to increase its catalytic activity in the hydrogen electrosorption/desorption reaction. The appropriate activation parameters were chosen on the basis of galvanostatic single-pulse curves recorded at the top of each hour after having soaked the alloy electrodes in a cold and afterwards in a hot 6 M KOH solution. It was proved, that each of the investigated electrodes achieved a minimal and stable resistance after 4 h activation at $T = 373$ K. Fig. 2 illustrates an example of the typical overpotential versus time curves for the III alloy electrode during the initial activation. The equilibrium potential of the electrode after activation is shifted towards the more negative values. The current versus potential dependence determined potentiodynamically in the vicinity of the equilibrium potential (Fig. 3) additionally proves the reversibility of hydrogen electrosorption/desorption after 4 h activation of the electrode at $T = 373$ K in 6 M KOH (see below).

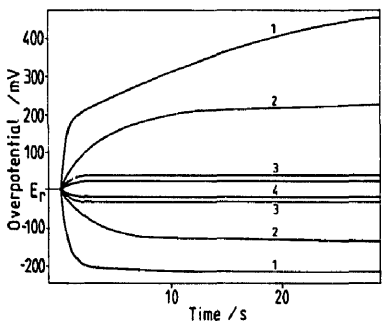

Fig. 2. Overpotential vs. time during anodic and cathodic galvanostatic pulses at $j = 40$ mA g^{-1} on the electrode made from alloy III: (1) after 24 h soaking in cold 6 M KOH, $E_r = -866$ mV; (2) after 1 h additional activation in 6 M KOH at $T = 373$ K, $E_r = -892$ mV; (3) after 2 h additional activation in 6 M KOH at $T = 373$ K, $E_r = -912$ mV, and (4) after 4 and 5 h additional activation in 6 M KOH at $T = 373$ K, $E_r = -918$ mV.

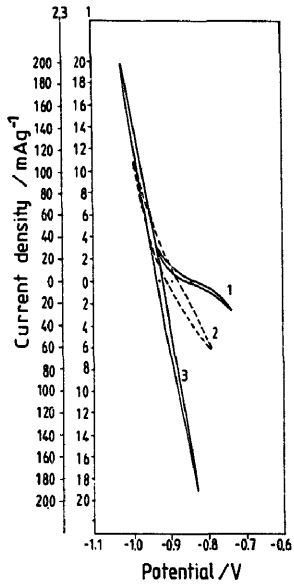

Fig. 3. Current density vs. potential for electrode made from alloy III, $v = 1$ mV s^{-1}: (1) after 24 h soaking in cold 6 M KOH, $E_r = -845$ mV; (2) after 2 h additional activation in 6 M KOH at $T = 373$ K, $E_r = -891$ mV, and (3) after 4 and 5 h additional activation in 6 M KOH at $T = 373$ K, $E_r = -926$ mV.

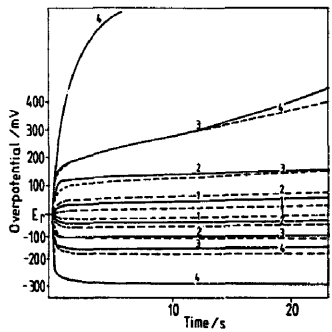

Fig. 4. Potential vs. time at various constant-current densities on chemically activated (———) compressed and (— — —) sintered electrode made of alloy V, during anodic and cathodic galvanostatic pulses at: (1) 40 mA g^{-1}; (2) 80 mA g^{-1}; (3) 160 mA g^{-1}, and (4) 320 mA g^{-1}.

3.2.2. Kinetics of hydrogen electrosorption/desorption

The kinetics of hydrogen electrosorption/desorption on the investigated alloys was estimated from the pulse and long-term galvanostatic as well as from potentiodynamic current–potential relations. Fig. 4 illustrates the overpotential versus time (η–t) dependence for compressed and sintered electrodes prepared from the chemically activated alloy V. It should be noted that the anodic and cathodic parts of these curves for both types of electrodes are symmetric with respect to the time axis at $j < 80$ mA g^{-1}. This means that the absolute overpotential value measured after any arbitrary period of time after the start of the galvanostatic pulse does not depend

on the current direction. Slight overpotential changes during the pulse duration indicate a high rate of the hydrogen diffusion in the solid phase of electrodes. It is typical of the reversible hydrogen electrosorption/desorption at alloy electrodes that the charge-transfer kinetics determines the overall rate of the electrode process.

The values of the charge-transfer resistance determined from extrapolation of the η–$t^{1/2}$ transient to $t=0$ and the $d\eta/j\,dt^{1/2}$ value, considered as a measure of changes in the diffusion resistance, are lower for the sintered electrode in comparison with those for the compressed ones. Furthermore, one can see in Fig. 4 that the symmetry of anodic and cathodic part of the η–t curves in the case of the sintered electrodes is maintained up to the current density of 160 mA g^{-1}. A decrease of the charge-transfer resistance and of the diffusion resistance was observed for all alloy electrodes in the charged state. For the discharged electrodes, the resistance increases again and the anodic and cathodic parts of the curve are not symmetric with respect to the time axis, especially at higher current densities. The differences in the galvanostatic performance of compressed and sintered electrodes as well as of charged and discharged ones prove that the kinetics of the hydrogen electrosorption/desorption is strongly affected by the surface state of the electrode material.

The reversibility of the hydrogen electrosorption/desorption on charged alloy electrodes under potentiodynamic conditions is shown in Fig. 5 and Fig. 6 by the typical current density versus potential (j–E) dependence, determined in the vicinity of the equlibrium potential E_r. For both the compressed and the sintered electrodes IV, in the charged state, the potential versus current dependence is linear with approximately the same slope of the anodic and cathodic branches

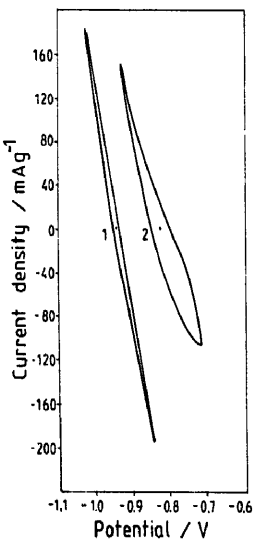

Fig. 5. Current density vs. potential for compressed electrode made from alloy IV in 6 M KOH in: (1) charged state, and (2) discharged state, $v=1$ mV s^{-1}.

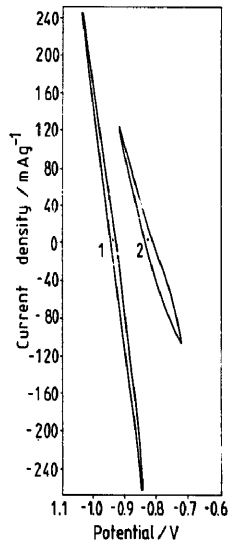

Fig. 6. Current density vs. potential for sintered electrode made from alloy IV in 6 M KOH in: (1) charged state, and (2) discharged state, $v=1$ mV s^{-1}.

in successive cycles. Because of the absence of any effect of the sweep rate (within 1–100 mV s^{-1}) on the current values, the slope coefficient of the j–E curves can be taken as the measure of charge-transfer resistance $R_{a(p)}=dE/dj$. It increases with the discharge depth of the electrode, which confirms the influence of the surface state of the alloy material on the kinetics of hydrogen electrosorption/desorption. An increase in the charge-transfer resistance and of the mass-transfer resistance at the end of electrode discharge could be explained in terms of a super-imposition of the oxidation of the absorbed hydrogen with the process of formation/dissolution of superficial oxides on the alloy particle surface.

The average values of charge-transfer resistance determined by means of the potentiodynamic ($R_{a(p)}$) and galvanostatic ($R_{a(g)}$) methods for electrodes I to V in charged state are compiled in Table 2. No significant differences in the charge-transfer resistance were found for the investigated electrodes. However, both the $R_{a(p)}$ and $R_{a(g)}$ values for the electrodes made of alloy V with Ti–Zr at the atomic ratio 1:1

Table 2
Average charge-transfer resistance of charged alloy electrodes determined by potentiodynamic $R_{a(p)}$ and galvanostatic $R_{a(g)}$ methods

Alloy	$R_{a(p)}$ ($\Omega\,g^{-1}$)		$R_{a(g)}$ ($\Omega\,g^{-1}$)	
	compressed electrode	sintered electrode	compressed electrode	sintered electrode
I	0.54		0.48	
II	0.53		0.41	
III	0.47		0.42	
IV	0.42	0.40	0.39	0.36
V	0.55	0.42	0.52	0.38

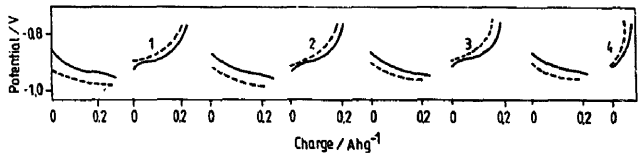

Fig. 7. Potential of compressed electrode made from (———) alloy IV and from (- - -) alloy V vs. charge upon cycling at $j = 40$ mA g^{-1} in: (1) 12th cycle; (2) 15th cycle; (3) in 25th cycle, and (4) after a 30-day storage at open circuit after charging to a depth of 100%.

are somewhat higher than that for the electrodes made of alloy IV for which the Ti:Zr ratio is 2:1. They are also higher for compressed electrodes than for the sintered electrodes made of the same alloy material.

3.2.3. *Influence of the alloy composition on the hydrogen-storage capacity*

The influence of alloy composition on the storage capacity for hydrogen absorption in successive charge/discharge cycles was tested in constant-current conditions, whereas the electrodes were charged to first symptoms of hydrogen evolution and discharged to −0.750 V potential versus Hg/HgO/6 M KOH.

Only a low storage capacity was found for electrodes made of alloys I to III, although the kinetics parameter for the hydrogen electrosorption/desorption measured under potentiodynamic and galvanostatic pulse conditions indicated the reversibility of hydrogen absorption/desorption. This capacity increases with decreasing manganese content and fluctuates from 40 mAh g^{-1} for alloy I to 80 mAh g^{-1} for alloy III. One can conclude that alloys with a high manganese content, instead of vanadium, are not useful as the MH electrode material without appropriate modification. The reason for such a behaviour might be a rapid dissolution of manganese from the electrode material in a strong alkaline solution, thus leading to undesirable changes in the electrode structure. This problem is expected to be overcome by micro-encapsulation of alloy particles [9–11]. Another way to receive the electrode material suitable for hydrogen battery appeared in decreasing the manganese content in an alloy.

As expected, high hydrogen-storage capacity and coulombic efficiency of the hydrogen electrosorption/desorption were obtained for the alloy electrodes IV and V containing about 7 at.% Mn. This is illustrated in Fig. 7 and Fig. 8 by the potential–time curves recorded during the long-term galvanostatic charge/discharge continuous cycling. The charge recovery for electrodes IV and V is nearly 90% at charging and discharging at appropriate current density, whereas the coulombic charge/discharge efficiency of alloy IV, containing less zirconium, is higher by about 10% or more than that of alloy V. This is in accordance with the lower charge-transfer and diffusion resistance for the first alloy as well as with the capacity differences derived from the electrochemical pressure–composition (*ep–c*) isotherms in Fig. 9. The electrochemical capacity of alloy V with increased zirconium content is smaller than that of alloy IV, while a reversed dependence is observed for hydrogen absorbed from the gas

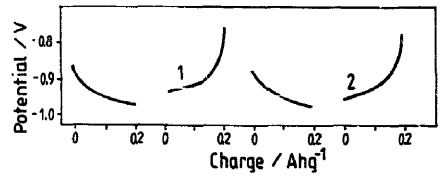

Fig. 8. Potential of sintered electrode made of alloy V vs. charge upon cycling at $j = 40$ mA g^{-1} in: (1) 15th cycle, and (2) 25th cycle.

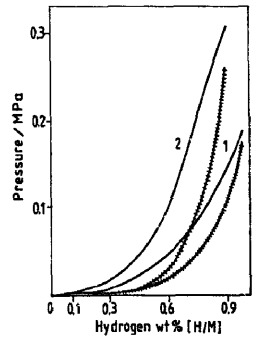

Fig. 9 Electrochemical pressure–composition isotherm (*ep–c*) for (——) absorption and (· · ·) desorption of hydrogen on: (1) compressed electrode made from alloy IV, and (2) compressed electrode made from alloy V, at 298 K.

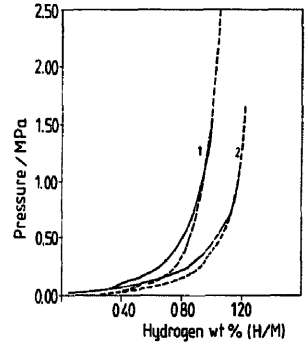

Fig. 10. Pressure composition isotherm (*p–c*) for (———) absorption and (— — —) desorption of hydrogen from the gas phase at room temperature on: (1) alloy IV, and (2) alloy V.

phase as shown by *p–c* isotherms in Fig. 10. Analogous regularities were obtained previously for alloys without manganese [4]. It might be explained by the differences in the

surface state of alloy particles in the electrode material in an alkaline solution and in the hydrogen atmosphere.

The discharge efficiency achieved for the sintered electrodes IV and V was lower (about 20 mAh g^{-1}) than that for the compressed ones. However, simultaneously these electrodes have a longer cycle life; no visible decrease in the discharge capacity was observed till 25th cycle (Fig. 8). On the other hand, the discharge capacity of compressed alloy electrodes decreases successively upon charge/discharge cycling. Most probably it is connected with the systematic, although slow dissolution of manganese from the electrode material in a strong alkaline solution. The sintering of electrodes containing manganese noticeably slows down this process.

Discharge capacities of the compressed electrodes made of alloys IV and V were, at the level of 230 and 210 mAh g^{-1}, slightly lower than that of other electrodes made of the AB_2 type material [4,6,12]. It is of about 80% of the theoretical capacity determined, as proposed by Anani et al. [13], on the basis of the hydrogen absorption/desorption isotherms measured in the gas phase (Fig. 10). The difference between the theoretical and the experimental capacity might originate not only from a manganese loss in the strong alkaline solution, but also from a poor contact between alloy granules as well as from the partial coverage of the surface of the electrode material by the oxide layer. The two latter undesirable phenomena, similarly as the manganese dissolution should be eliminated or at least limited by covering the alloy with a thin appropriate metallic layer (micro-encapsulation [9–11]). This procedure should lead to an increase in the capacity and cycle life of the alloy electrode. The capacity loss of about 60% for compressed electrodes IV and V during storage determined in the charge-retention tests after 30 days storage in open circuit at $T = 298$ K (Fig. 7) confirm the necessity of the modification of the electrode material. The studies on the subject are in progress.

4. Conclusions

An appropriate chemical activation of the multicomponent Zr–Ti–V–Mn–Cr–Ni alloys in 6 M KOH solution at 373 K causes an increase in the catalytic activity of electrode material. At appropriate V:Mn ratio, the alloy electrode reveals a relatively high discharge capacity, yet is unstable upon cycling. Sintering of alloy electrodes reduces its dissolution in electrolyte. Further restriction of manganese dissolution is expected to be achieved by micro-encapsulating. Electrodes with an increased Ti:Zr atomic ratio, 2:1, display higher hydrogen-storage capacity than electrodes containing titanium and zirconium at the ratio 1:1. The catalytic activity of the former alloys is also higher (charge-transfer and diffusion resistances lower). This could be explained by an increased resistance to oxidation of the alloy surface or in terms of the proper interaction between alloy components, resulting in an synergistic effect.

This work was sponsored by Komitet Badań Naukowych, Poland, within research project No. 8.5502 083 04.

Acknowledgements

The authors thank Professor Dr hab. H. Drulis (Institute of Low Temperature and Structure Research, Polish Academy of Sciences, Wrocław) for kindly supplying the alloy samples characterized by gas-phase isotherms.

References

[1] S. Venkatesan, M.A. Fetcenko, B. Reichman, D. Magnuson and S. Dhar, *Proc. 2nd Int. Rechargeable Battery Seminar, Deerfield Beach, FL, USA, 7–9 Mar. 1988.*

[2] M.A. Fetcenko, S. Venkatesan, K.C. Hong and B. Reichman, *J. Power Sources, 12* (1988) 411.

[3] B. Reichman, S. Venkatesan, M.A. Fetcenko, K. Jeffries, S. Stahl and C. Bennet, *US Patent No. 4 716 088* (29 Dec. 1987).

[4] M. Kopczyk, G. Wójcik, G. Młynarek, A. Sierczyńska and M. Bełtowska-Brzezinska, *J. Appl. Electrochem.*, in press.

[5] C. Iwakura, T. Asaoka, H. Yoneyama, T. Sakai, K. Oguro and H. Ishikawa, *Nippon Kagaku Kaishi*, 1988 (1988) 1482.

[6] H. Miyamura, T. Sakai, N. Kuriyama, K. Oguro, A. Kato and H. Ishikawa, in A.D. Corrigan (ed.), *Proc. Symp. Hydrogen Storage Materials, Batteries and Electrochemistry*, Proc. Vol. 5, The Electrochemical Society, Pennington, NJ, USA, 1992, p. 179.

[7] B.K. Zoitos, D.L. Hudson, P.D. Bennett and V.I. Puglisi, in A.D. Corrigan (ed.), *Proc. Symp. Hydrogen Storage Materials, Batteries and Electrochemistry*, Proc. Vol. 5, The Electrochemical Society, Pennington, NJ, USA, 1992, p. 168.

[8] C. Iwakura, M. Matsuoka, K. Asai and T. Kohno, *J. Power Sources, 38* (1992) 335.

[9] M. Matsuoka, K. Asai, K. Asai, Y. Fukumoto and C. Iwakura, *J. Alloys Comp., 192* (1993) 149.

[10] H. Ishikawa, K. Oguro, A. Kato, H. Suzuki and E. Ishii, *J. Less-Common Met., 120* (1986) 23.

[11] K. Naito, T. Matsunami, K. Okuno, M. Matsuoka and C. Iwakura, *J. Appl. Electrochem., 24* (1994) 808.

[12] M. A. Fetcenko and S. Venkatesan, *Prog. Batteries Solar Cells, 9* (1990) 259.

[13] A. Anani, A. Visintin, S. Srinivasan, A.J. Appleby, J.J. Reilly and J.R. Johnson, in A.D. Corrigan (ed.), *Proc. Symp. Hydrogen Storage Materials, Batteries and Electrochemistry*, Proc. Vol. 5, The Elecrtrochemical Society, Pennington, NJ, USA, 1992, p. 105.